Journal of Physics: Condensed Matter

PAPER

Tunable tunnel barriers in a semiconductor via ionization of individual atoms

To cite this article: Sara M Mueller *et al* 2021 *J. Phys.: Condens. Matter* **33** 275002

IOP Publishing Journal of Physics: Condensed Matter
J. Phys.: Condens. Matter **33** (2021) 275002 (9pp) https://doi.org/10.1088/1361-648X/abf9bd

Tunable tunnel barriers in a semiconductor via ionization of individual atoms

Sara M Mueller[1], Dongjoon Kim[2], Stephen R McMillan[3], Steven J Tjung[1], Jacob J Repicky[1], Stephen Gant[1], Evan Lang[1], Fedor Bergmann[4], Kevin Werner[1,5], Enam Chowdhury[1,6], Aravind Asthagiri[2], Michael E Flatté[3] and Jay A Gupta[1,*]

[1] Department of Physics, Ohio State University, Columbus, OH 43210, United States of America
[2] Department of Chemical and Biomolecular Engineering, Ohio State University, Columbus, OH 43210, United States of America
[3] Department of Physics and Astronomy, University of Iowa, Iowa City, IA 52242, United States of America
[4] Bergmann Messgeraete Entwicklung KG, Kocheler Strasse 101, 82418 Murnau, Germany
[5] BAE Systems, 130 Daniel Webster Hwy., MER15-1813, Merrimack, NH 03054, United States of America
[6] Department of Material Science and Engineering, Ohio State University, Columbus OH 43210, United States of America

E-mail: Gupta.208@osu.edu

Received 30 December 2020, revised 30 March 2021
Accepted for publication 20 April 2021
Published 28 May 2021

Abstract

We report scanning tunneling microscopy (STM) studies of individual adatoms deposited on an InSb(110) surface. The adatoms can be reproducibly dropped off from the STM tip by voltage pulses, and impact tunneling into the surface by up to $\sim$100$\times$. The spatial extent and magnitude of the tunneling effect are widely tunable by imaging conditions such as bias voltage, set current and photoillumination. We attribute the effect to occupation of a (+/0) charge transition level, and switching of the associated adatom-induced band bending. The effect in STM topographic images is well reproduced by transport modeling of filling and emptying rates as a function of the tip position. STM atomic contrast and tunneling spectra are in good agreement with density functional theory calculations for In adatoms. The adatom ionization effect can extend to distances greater than 50 nm away, which we attribute to the low concentration and low binding energy of the residual donors in the undoped InSb crystal. These studies demonstrate how individual atoms can be used to sensitively control current flow in nanoscale devices.

Keywords: scanning tunneling microscopy, semiconductor dopants, single dopant ionization, surface photovoltage, InSb

S Supplementary material for this article is available online

(Some figures may appear in colour only in the online journal)

1. Introduction

As electronic devices miniaturize to the nanometer scale, their performance and reproducibility becomes increasingly impacted by single-impurity effects [1–3]. Nanoscale electronics, such as single atom transistors [4], are a realization of a new 'solotronics' [5], where control and manipulation of individual impurity atoms in a material determines the device performance. In this context, the scanning tunneling microscope (STM) has been used for deterministic placement of

* Author to whom any correspondence should be addressed.

dopants [4, 6] and to tune dopant binding energies via control of the local electrostatic environment [7]. STM-induced ionization is also a promising demonstration for control, and has now been reported in various systems including dopants in III–V's [8–12], silicon dangling bonds [13–17], C_{60} [18], cobalt on graphene [19], iron on Bi_2Se_3 [20] and vacancies in ZnO [21].

Here we report a tip-induced ionization effect that reveals how individual adatoms can be used to tune the tunneling conductance of an InSb(110) surface by two orders of magnitude over relatively large areas. When the adatoms are in a positive charge state, adatom induced band bending leads to a high-conductance accumulation region that can extend for $\gg$100 nm^2 due to the very low binding energy of native donors in InSb. Under certain imaging conditions, the adatom can be switched to a neutral state by a tunneling electron from the STM tip, leading to a low-conductance depletion region appearing as a 'crater' feature in topographic STM images. The crater size can be tuned with bias voltage, set current, and photoillumination. The experimental results are confirmed by comparisons with DFT calculations and theoretical transport modeling. These studies provide insight into how single atoms can be harnessed in future nanoscale opto/electronic devices.

2. Methods

Experiments were conducted in a Createc LT-STM at 5 K in ultrahigh vacuum ($< 10^{-10}$ mbar) using electrochemically etched Pt/Ir tips with an apex diameter $<$ 500 nm. The InSb sample was a commercial bulk wafer, nominally undoped, but with *n*-type conductivity verified with Hall effect measurements. Typical donor species (e.g., S, Se, Te) in InSb are thought to occur at a concentration in the 10^{13-14} cm^{-3} range, with a ∼0.6 meV binding energy [22, 23]. The sample was cleaved at ∼100 K in UHV, exposing the (110) surface, immediately before transfer into the STM. Tunneling spectroscopy was performed by adding a 10 mV modulation to the sample bias. A lock-in detects the corresponding dI/dV (V) signal, which is related to the local density of states (LDOS). To tune band bending via the surface photovoltage (SPV) effect [19], light from a home-built laser (1550 nm, 125 fs pulses at a 70 MHz repetition rate) was aligned to a side viewport on the STM chamber. An average laser power of 1.5 mW was directed at glancing incidence onto the sample with no additional focusing. The illuminated area on the sample was relatively large (∼0.5 cm^2), so that careful alignment of laser and tip was not necessary.

All plane wave DFT calculations were performed using the projector augmented wave pseudopotentials provided in the Vienna *ab initio* simulation package (VASP) [25–27]. Further details of the calculations are provided in the supporting information (https://stacks.iop.org/JPCM/33/275002/mmedia), but here we note that the bulk InSb band gap with Perdew–Burke–Ernzerhof (PBE) [31] is more accurate than the hybrid HSE06 functional [32] value. Based on this result we chose the PBE functional for all InSb(110) surface calculations reported in the paper. Surface relaxation was performed with the lateral dimensions fixed to the bulk PBE lattice constant, a force criteria of 0.03 eV Å^{-1}, a plane wave cutoff of 400 eV and Γ-centered 4 × 4 × 1 *k* grids. We tested the four most likely adatom candidates (In, Sb, Pt, Ir) on the site indicated by the STM images. Bader charge analysis [28] was performed for each of the adatom candidates using the program from Henkelman and co-workers [29–31]. We obtain LDOS of the In adatom and bare InSb surface using the same settings (*k*-point grid, plane wave cutoff) as for the bare surface relaxation. Lastly, we simulated constant-height STM images of adatoms on the InSb surface using the Tersoff–Hamman model [32] for both empty and filled state conditions using the p4vasp software package [33].

3. Results and discussion

Figure 1(a) shows an STM image of the clean InSb(110) surface under filled-state imaging conditions where the rows of Sb atoms are resolved [34], as are a few bright features which correspond to a low coverage of molecular adsorbates from the UHV chamber. Larger scale images of the surface (figure S1) show very few native defects such as surface/sub-surface dopants or atomic vacancies, which we attribute to the low defect concentration in our sample. During tip forming procedures (e.g., approach, voltage pulsing) that are typically used to sharpen STM tips, we were able to produce new point defects on the surface that we attribute to individual adatoms. For example, figure 1(b) shows the same area as figure 1(a) after pulsing the bias voltage to ∼+8 V for 0.5 s, which dropped an adatom off the tip. This process was reproducible, although the conditions for dropping adatoms off vary with the microscopic details of the tip apex, which are not well characterized and can change during the course of the experiments. We attribute these defects to individual adatoms based on their small apparent size and reproducible appearance. If the tip were depositing few-atom clusters, we would expect variations in number, size and shape of the features that were not observed in the experiment.

We attribute the defect in figure 1(b) to an In adatom dropped off from the tip based on a comparison of our experimental data with DFT calculations. Similar atomic manipulation was previously reported for In_{ad} on reconstructed InAs(111)A surfaces [35–37], and for Ga_{ad} on GaAs(110) surfaces [23]. In our prior work on GaAs, we found that the STM tip readily becomes terminated with the substrate material during standard tip forming procedures, and we could deposit Ga adatoms in a similar fashion. Discussed further in supporting information, we first determined the adatom adsorption site from atomic resolution images where both In and Sb atomic rows could be identified (cf, figure 1(c)). We then performed DFT calculations of the four most likely candidates (i.e., In, Sb, or Pt/Ir from the tip) on this and other high symmetry sites. Bader charge analysis was used to estimate the charge state of the adatoms, and we find that of the four candidates on this site, only In_{ad} is positively charged, which agrees with the experimentally determined charge discussed below. The DFT-simulated STM image for In_{ad} (figure 1(d)) is in reasonable qualitative agreement with experiment (figure 1(c)),

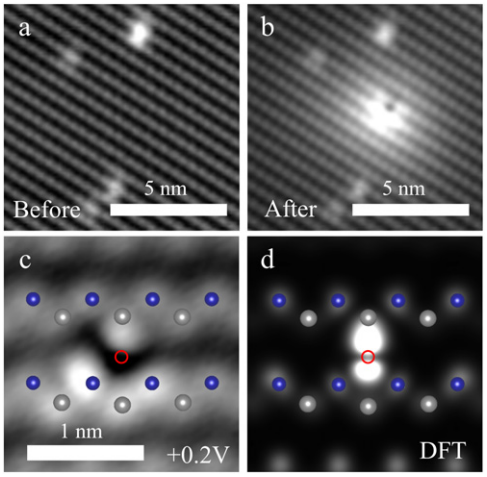

Figure 1. Adatom deposition and binding site assignment. STM topographic images (a) before and (b) after a voltage pulse deposited an adatom to the InSb(110) surface ($V = -0.5$ V, $I = 0.22$ nA). (c) Magnified view of adatom with InSb lattice overlay, blue atoms are Sb, gray are In, red circle is adatom site inferred from DFT ($V = +0.2$ V, $I = 0.22$ nA). (d) DFT simulated STM image using a bias voltage of +0.3 V. Red circle indicates the adatom position.

reproducing the enhancement of contrast along the neighboring Sb row (similar to a previous study of Fe_{ad} on InSb [39]), and the dark node centered on the atomic site. In further support of this assignment, we find good agreement between experimental and calculated LDOS for the In adatom (cf, figure 5), and include additional discussion in the supporting information demonstrating instances where the adatoms could be picked up, or where adatom/vacancy pairs were generated, either from cleavage at lower temperature or STM pulsing.

We now discuss the charge state of the adatom and tip-induced ionization effects. Figure 2 shows that the adatom images as a protrusion at negative bias (figure 2(a)), and as a dark 'crater' feature at positive bias (figure 2(b)). Linecuts of the apparent topography as indicated in these images are shown in figure 2(c). At negative bias, the apparent topography shows a gradual fall-off that extends for several nm away from the adatom site, much further than the atomic states associated with the adatom. This is commonly observed for charged species on III–V (110) surfaces where the absence of in-gap surface states leads to reduced screening, and we attribute the change in topography to adatom-induced band bending (AIBB) of a positive point charge [38, 40]. To understand this connection, we note that the tunneling probability (and thus apparent height in STM images) depends on the total potential at the surface underneath the tip which is the sum of several contributions as given by equation (1):

$$V_{\text{total}}(r, z=0) = V_{\text{tip}}(V, z, ..) - \frac{Q_{\text{ad}}}{4\pi(\varepsilon_{\text{InSb}}/2)\varepsilon_0 r} - \sum_{1}^{N} \frac{Q_i}{4\pi\varepsilon_{\text{InSb}}\varepsilon_0 r_i} \mp N(h\nu, I_0). \quad (1)$$

Here, the first term on the right-hand side represents tip induced band bending (TIBB) which is a function of bias voltage V, tip height z (and other tip parameters), and switches sign at $V = V_{\text{FB}}$, where V_{FB} is the flat band voltage. The second term represents AIBB due to the adatom Coulomb potential (with charge Q_{ad}) and accounting for a reduced effective dielectric constant at the surface ($\varepsilon_{\text{InSb}}/2$). The third term represents the potentials from any other ionized dopants nearby, which we will neglect here due to the low defect concentration in our samples. The last term represents the SPV contribution when the sample is being illuminated at energy $h\nu$ and intensity I_0. The separation of photo-excited carriers in local electrostatic fields always acts to decrease the total potential regardless of its sign [24], and the underlying dynamics can be spatially resolved near individual impurities [41]. Though it is difficult to determine TIBB directly, we performed a number of simulations using the SEMITIP Poisson solver from Feenstra [42] to estimate TIBB using typical values of tip sharpness, work function and bias voltage, which is discussed further in the supporting information. Based on the electron affinity of InSb and the estimated work function for the PtIr tips, we expect the flat band condition to be in the range $-0.2V < V_{\text{FB}} < 0.4V$ in our experiments.

The tunneling diagrams in figures 2(a) and (b) describe how the image contrast reflects the adatom charge state, which depends on the tip distance. Under the filled-state imaging conditions in figure 2(a), we expect TIBB < 0, which should cause an accumulation of conduction electrons under the tip in our n-type sample [12]. This accumulation region moves in concert with the tip, and while tunneling of these electrons into the tip's empty states affects the absolute tip-sample distance, it is largely invisible in the experimental images. The bright contrast near the adatom is consistent with a positive adatom charge state; AIBB < 0 increases accumulation near the adatom (green bands and arrow in figure 2(d)) and the tip moves further from the surface in the constant-current image [40, 43]. The gradual fall-off in figure 2(c) is consistent with a screened Coulomb potential [17], with a screening length of ~ 3.5 nm that depends on the imaging conditions through TIBB (V, z) (cf, supporting information). Adatom-induced accumulation reflects charge transfer upon adsorption, and at higher coverages, produces surface-confined 2D electron gases as shown on n-InSb(110) [44] and InAs(110) [45]. Similar to the In_{ad}/InAs(111)A system [36, 37], the In adatom in our studies acts like a 'surface donor' and the associated (+/0) charge transition level must lie above the conduction band edge for the adatom to be remain positively charged under all filled-state imaging conditions.

Under empty state imaging as in figure 2(b), the crater feature shows an abrupt change in apparent height of 150 pm, indicating more than a tenfold reduction in tunneling conductance. The Sb rows are observed within the crater feature and appear continuous with the rows outside of the crater, indicating this is an electronic effect rather than a true topographic feature. The bottom of the crater is relatively flat (figure 2(c), blue curve), and there is no longer-range fall off in apparent height near the adatom position, suggesting that the adatom is now in a neutral charge state. With $V > V_{\text{FB}}$ and thus TIBB > 0, tunneling electrons from the tip must cross a depletion barrier to get to empty states in the InSb conduction band.

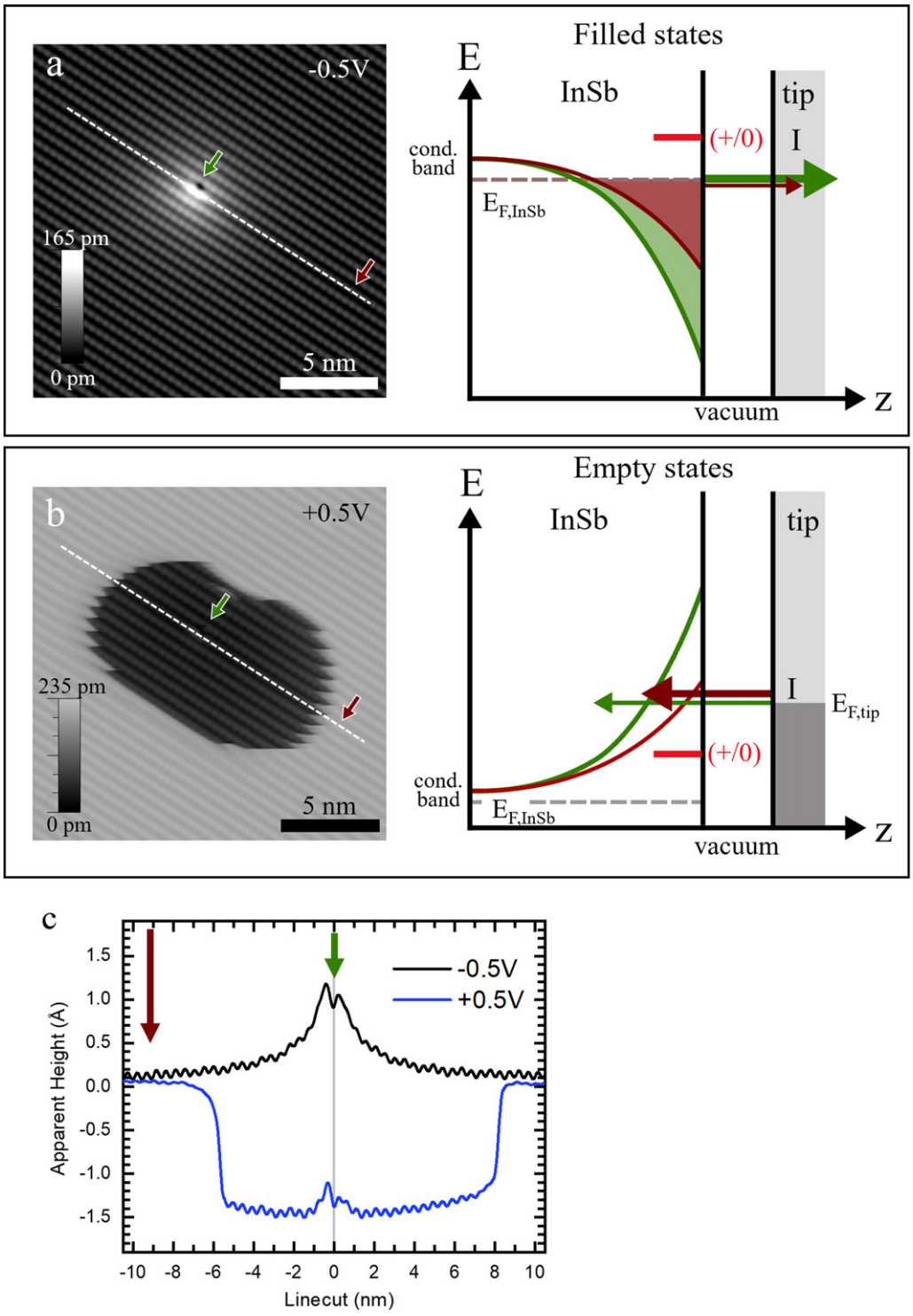

Figure 2. STM-induced switching of adatom charge state (a) adatom under negative bias conditions (filled states) images as a protrusion ($V = -0.5$ V, $I = 0.22$ nA). Accompanying tunneling diagram shows tunneling of electrons accumulated under the tip (solid regions). As the tip approaches the adatom (green), the additional accumulation from AIBB < 0 increases the tunneling probability compared to far from the adatom (brown). (b) A dark 'crater' appears under positive bias imaging (empty states) ($V = +0.5$ V, $I = 0.22$ nA). When the tip is far from the adatom (brown arrow), AIBB < 0 but TBB > 0 and electrons tunnel from the tip into the InSb conduction band as shown by the brown arrow in the accompanying tunneling diagram. Once a tunneling electron occupies the (+/0) adatom level (red dotted arrow), AIBB $= 0$ and increased TBB leads to a depletion barrier for tunneling electrons (green arrow). (c) Topography linecuts indicated by the dotted lines in (a) and (b) showing a 1.5 Å change in apparent height associated with the crater feature.

This depletion region also follows the tip as it is scanned, and is not readily apparent in STM imaging of the bare InSb surface. When the STM tip approaches within a threshold distance of the adatom (red arrow in figure 2(b)), the adatom switches to a neutral charge state. This leads to an abrupt increase in the total potential as AIBB $\rightarrow 0$ and thus leads to an increased depletion barrier near the tip (green curve in figure 2(b)). As a result, the tip must get significantly closer to the surface to maintain a constant current, accounting for the apparent depth of the crater feature. Discussed further in the supporting information, we found that crater features were reproduced using STM tips with different atomic terminations and in constant height imaging mode, however, the detailed shape and other characteristics such as apparent depth and current/voltage dependence vary with the tip termination.

We note that the change in the adatom charge transition level relative to the InSb conduction band edge implied in figures 2(a) and (b) is quite different from what would be expected from a conventional dopant in the bulk of a semiconductor. In contrast to a dopant transition level, whose wave function is entirely within the semiconductor, here the adatom's wave function is predominately within the vacuum external to the semiconductor, and hence the charge-transition level should be predominately fixed relative to the vacuum. In contrast, the relative energy of the semiconductor bands at the surface with respect to the vacuum is changing under these different imaging conditions due to the TIBB and resulting charge accumulation at the surface. We also note that fixed energy levels with respect to vacuum have been reported for dopants within the top layer of a semiconductor surface [7], hydrogen within a series of semiconductors [46] and for 'hyperdeep' trap states within the bulk [47].

The abrupt change in charge state as the tip approaches the adatom is suggestive of a tip-induced ionization effect. Recently, disk- or ring-like features in STM images of impurities in other III–V semiconductors have been attributed to the ionization of individual dopants at a threshold value of TIBB that brings a dopant charge transition level into resonance with the host Fermi level [8, 9, 11]. The size and shape of these features depend on factors which affect TIBB, including bias voltage, set current and the tip apex structure.

In figure 3 we demonstrate a similar tunability of the crater feature, although we find that an alternate ionization mechanism is necessary to consistently explain all the data. Compared to the crater under typical imaging conditions (figure 3(a)), we observed a significant reduction in size by three methods: (i) illuminating the sample with light (figure 3(c)), (ii) reducing the set tunneling current (figure 3(d)), and (iii) increasing the bias voltage (figure 3(b)). Under illumination, SPV counteracts TIBB, and the tip must move closer to the adatom to achieve the same threshold condition. Similarly, a reduced set current (figure 3(d)) moves the tip further from the surface and thus reduces TIBB, which shifts the threshold condition closer to the adatom as well.

While observations (i) and (ii) are qualitatively consistent with a resonance TIBB ionization effect, the sensitivity of the crater to such small changes in set current and (iii) the *reduction* of the crater size with higher positive voltage (figure 3(b)) suggests an alternative mechanism is needed. Because TIBB monotonically increases with voltage from $+0.5$ V (figure 3(a)) to $+0.9$ V (figure 3(b)), the threshold condition should be met at a larger tip-adatom distance (i.e., larger crater), in contrast to the observation. In the supporting information, we considered other possible scenarios given our uncertainties in V_{FB} and other TIBB parameters. Our conclusion is that there is no resonance TIBB scenario that explains the trends in crater size with V, I while also being consistent with our assignment of a positive charge state when the tip is far away from the adatom, and a neutral charge state when the tip is brought nearby.

Following an approach developed for STM tip-induced ionization of dangling bonds in silicon [13, 14, 16], we propose a competing rate model and find good qualitative agreement between our observations and theoretical transport modeling (figure 4). Here, TIBB > 0 raises the InSb conduction band so that the adatom's $(+/0)$ charge transition level lies in a double-barrier configuration, resembling a quantum dot coupled to two leads [14]. Our model includes one channel for the tunneling current characterized by a filling rate from the tip, Γ_{f}, and an emptying rate into the bulk, Γ_{e}. Once the adatom state is filled by an electron from the tip tunneling through the vacuum barrier, it must escape into the bulk by tunneling through a surface depletion barrier, with a height and width that depend on TIBB. The time-averaged occupation of the state is given by $N = \frac{\Gamma_{\mathrm{f}}}{(\Gamma_{\mathrm{f}}+\Gamma_{\mathrm{e}})}$ and reaches a value of 1/2 when $\Gamma_{\mathrm{f}} = \Gamma_{\mathrm{e}}$. Direct tunneling into the InSb surface is considered as a second tunneling channel, with rates Γ_0, Γ_1 that depend on the adatom charge state (neutral and positive respectively) via AIBB.

Of these four rates, we can estimate Γ_0, Γ_1 from tunneling into InSb with the tip positioned inside/outside the crater region, and we calculate $\Gamma_{\mathrm{f}}(r)$ using a Tersoff–Hamann approximation treating the terminating tip atom as a spherically symmetric wavefunction, and the adatom wavefunction with separate vertical (z_0) and lateral (r_0) decay constants. The filling/emptying rates are difficult to directly estimate from our STM data because they are sensitive to the measurement conditions and can easily lie outside the limited instrumental bandwidth ($\sim$1 kHz), but we note that 'telegraph' noise is observed in STM images under certain conditions that is suggestive of these dynamics.

Figure 4 shows a plot of the apparent height at constant current from this calculation as a function of the lateral separation between tip and adatom. As shown in the figure, the apparent height transitions from a low to high value as the tip moves laterally away from the adatom. The transition reflects the threshold separation where $\Gamma_{\mathrm{f}} \sim \Gamma_{\mathrm{e}}$. For $\Gamma_{\mathrm{e,f}} \sim 10$ kHz (black curve in figure 4(b)), our calculations predict that the transition should occur at a separation of $\sim$5 nm, which is in qualitative agreement with the experimental image in figure 3(a). Applying this model now to the trends in figure 3, we note that under photoillumination, the width of the depletion barrier decreases, which increases Γ_{e} but has no direct effect on Γ_{f}. The tip must therefore approach laterally closer to the adatom to balance the filling and emptying rates, consistent with the reduced crater size in figures 3(c) and 4(b) (green curve). Reduction of set

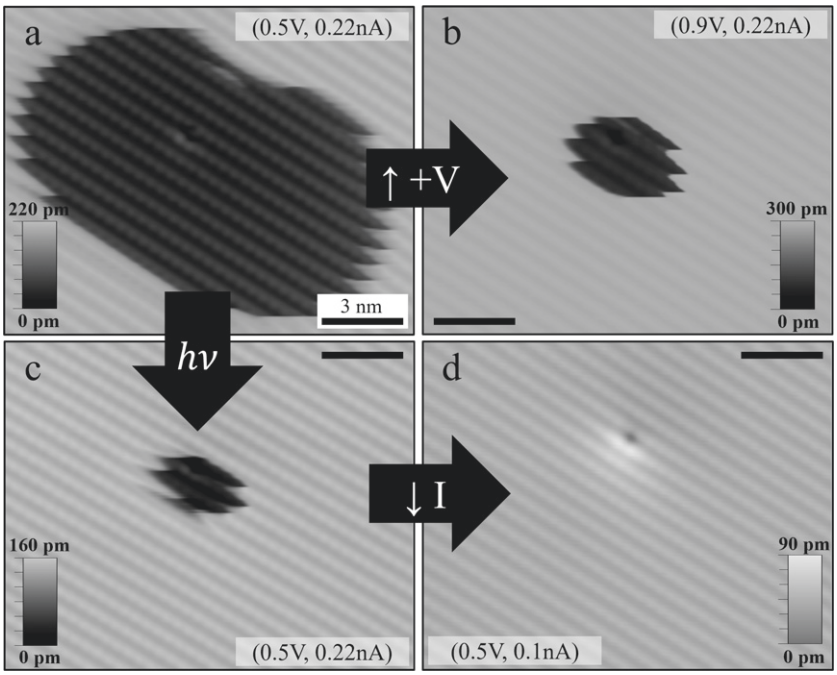

Figure 3. Tuning of crater effect. (a) STM image showing a crater feature under typical imaging conditions (+0.5 V, 0.22 nA). The crater size decreases (i.e., the tip must get laterally closer to the adatom to maintain occupation of the (+/0) level) by: (b) increased voltage (+0.9 V, 0.22 nA) or (c) photoillumination (+0.5 V, 0.22 nA) and (d) subsequent decrease in set current (+0.5 V, 0.17 nA). All scale bars are 5 nm.

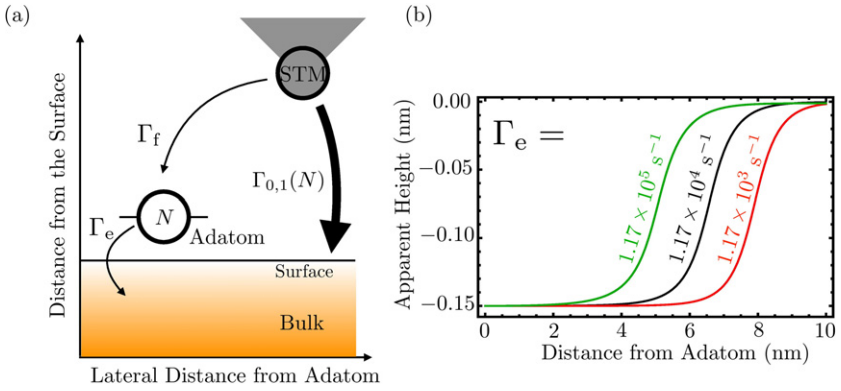

Figure 4. Rates modeling. (a) Schematic showing tunneling channels through the adatom level and directly into the bulk. The total current is dominated by tunneling directly into the bulk as indicated by the weight of the arrows. Occupation of the (+/0) adatom level determines the magnitude of the bulk tunneling rate (Γ_0 or Γ_1) and is governed by the filling rate, Γ_f, and emptying rate, Γ_e. (b) Calculated apparent height based on the two-channel electrical transport model plotted for different values of Γ_e. For kHz-scale emptying rates, a change in apparent height occurs with the tip several nm away, qualitatively consistent with experiment.

current directly decreases Γ_f, so that the tip must move laterally closer to the adatom to increase the depletion barrier width and decrease Γ_e, consistent with figure 3(d). Higher positive voltage affects both rates with opposite effects on crater size: Γ_e decreases because of a wider depletion barrier, while Γ_f decreases because tunneling electrons from the tip have a higher vacuum barrier into the adatom state (neglecting the possibility of inelastic electron tunneling). Reduction in Γ_f decreases the crater size while a reduction in Γ_e increases the crater size. The data in figure 3(b) are consistent with a net reduction in the Γ_f/Γ_e ratio at higher positive voltage: the tip must approach laterally closer to the adatom to increase Γ_f and achieve the threshold condition, resulting in a smaller crater. Further discussion of the model presented in figure 4 can be found in supporting information.

To identify the adatom charge transition level responsible for the ionization crater, we compared tunneling spectroscopy data with the tip positioned on pristine InSb (figure 5(a), black) and the adatom (figure 5(a), red). Though TIBB complicates a precise measurement of the gap in STM studies of semiconductors [48], on InSb, there is a minimum in the measured dI/dV signal in the range ±200 mV that roughly reflects the InSb band gap of 235 meV. The rise in conductance starting in the range 0 → +150 mV is attributed to the InSb conduction band, and the more gradual rise below −200 mV reflects the valence band. Tunneling spectroscopy

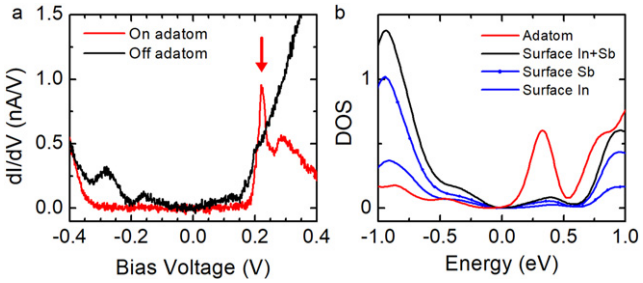

Figure 5. Identification of the adatom charge transition level (a) dI/dV spectroscopy on (red) and off (black) adatom showing a peak at 250 mV (red arrow) attributed to the (+/0) charge transition level of the adatom. (b) DFT-calculated LDOS for the indium adatom (red), as well as surface In atoms (blue), surface Sb atoms (dashed) and combined In and Sb atoms (black).

on the adatom (figure 5(a), red) indicates enhanced conductance below −400 mV consistent with increased accumulation due to AIBB < 0, and a pronounced suppression of the conductance above ∼300 mV, consistent with tunneling through a depletion region when AIBB $= 0$. We interpret the peak at +250 mV as the (+/0) charge transition level, which importantly lies above the InSb conduction band edge and E_F. This suggests the level is unoccupied and the adatom is in the + charge state in the absence of the tip and at negative bias, consistent with the bright topographic contrast in figure 2(a). At large positive bias, the adatom is maintained in the neutral state by electrons tunneling from the tip into the adatom level. The tunneling spectra are also in good agreement with the DFT-calculated LDOS. The InSb(110) surface DOS (figure 5(b), black) shows a minimum around 0 eV reflecting the band gap, and no prominent peaks in the range ±500 meV. In contrast, the In adatom density of states (figure 5(b), red) show a distinct peak above the conduction band edge near +250 meV, and this is not present in the calculated DOS of the surface indium sites (figure 5(b), blue).

Somewhat counterintuitively, the spatial extent of the crater feature sets a *lower* limit for the length scale over which the adatoms influence the tunneling conductivity of the InSb(110) surface. Because the crater corresponds to the region where AIBB $= 0$, the apparent height of the surface *outside* the crater must reflect AIBB $\neq 0$, or there would be no change in contrast due to the adatom charge state. To estimate the limit of the spatial extent, we show in figure 6 a series of images as a function of voltage with a few adatoms deposited from the tip. With a modest decrease in bias voltage, the crater features eventually grow to exceed the entire scan area, indicating that individual adatoms influence the surface conduction over distances greater than 50 nm. We attribute the additional suppression of conductance on the left in figure 6(c) to filling from a point on the tip distinct from the tunneling apex. Although these points are further from the surface and do not contribute much to Γ_0, Γ_1, they can be closer to the adatom and have higher Γ_f. This behavior further distinguishes ionization in the competing rates model [14–16, 49] from the resonant TIBB models [8, 9, 11].

We attribute the remarkable spatial extent of the adatom-tunable conductance to the low concentration and binding

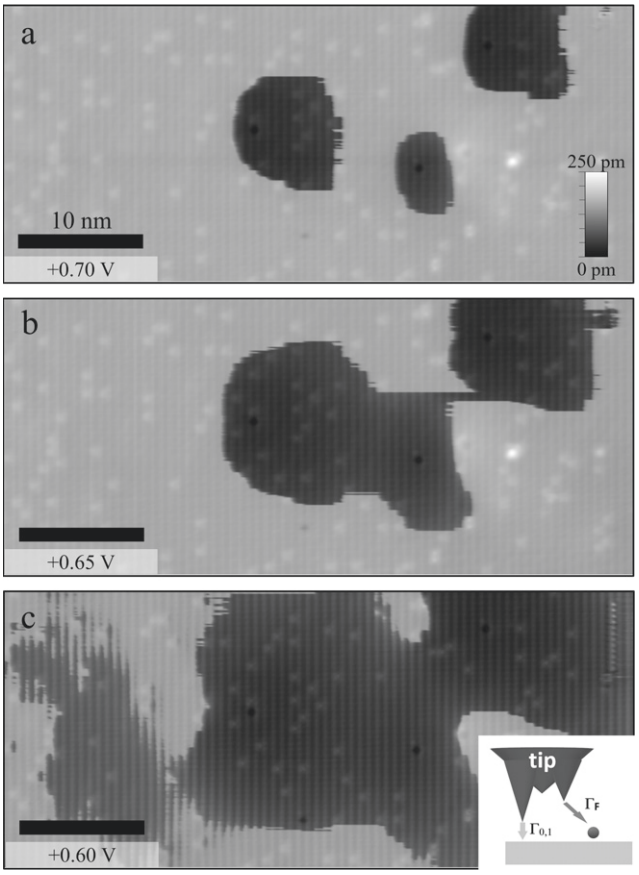

Figure 6. Crater expansion. (a) Three crater features localized to their respective adatoms. (b) With a modest reduction in bias voltage, craters expand and overlap. (c) Further reduction shows more overlap and development of an 'auxiliary crater' attributed to tunneling electrons into the adatom from higher up on the tip (I = 0.22 nA). Scale bars are 10 nm.

energy (∼ 0.6 meV) of the residual donors in the undoped InSb crystal [22]. This ionization energy is comparable to $k_BT \sim 0.4$ meV at 5 K, which suggests that a sizable fraction of the donors can be readily ionized thermally or by the electrostatic potentials of individual adatoms. Indeed, the Coulomb potential for a $+e$ adatom falls below 0.6 meV at a distance of ∼140 nm, assuming an effective static dielectric constant of $\varepsilon = 16.8$ for bulk InSb. This sensitivity distinguishes the ionization effect observed here from previous studies and suggests that undoped semiconductors with a low concentration of very shallow dopants may be well suited for future solotronic devices.

4. Conclusions

In this work we demonstrated tunability of the conductance of the InSb(110) surface by individual indium adatoms. Our experimental data are found to be in good agreement with DFT calculations and a transport model considering adatom and bulk tunneling channels. Similar effects to those described above were observed at step-edges and near larger nanoclusters that were occasionally deposited onto the surface during tip-forming, suggesting this is a more general phenomenon

that is not specific to the particular adatom species. STM-based pulse methods as demonstrated recently for the Si dangling bonds [16, 49] would allow for direct correlation of tunneling rates with the local environment, thus providing a microscopic picture of electronic transport.

Acknowledgments

SMM performed TIBB simulations, STM measurements, and data analysis. ST, and JR performed STM measurements. SG, DK and AA performed the DFT calculations. SRM and MEF performed the transport modeling. EL, FB, KW and EC built and characterized the laser used for SPV measurements. All authors reviewed the manuscript and contributed to the writing of the text. We acknowledge support from the Department of Energy under Grant #DE-SC0016379. Laser construction and characterization by (EL, FB, KW, EC) was funded by a Grant from AFOSR (Grant #FA9550-12-1-0454). EC and KW acknowledges support from AFOSR Grant FA9550-16-1-0069, and AFRL Grant FA9451-14-1-0351. AA and DK were supported by NSF #1809837 and acknowledge the Ohio Supercomputing Center for providing computational resources.

Data availability statement

The data that support the findings of this study are available upon reasonable request from the authors.

ORCID iDs

Stephen R McMillan https://orcid.org/0000-0001-8544-6316
Aravind Asthagiri https://orcid.org/0000-0001-5301-1246
Michael E Flatté https://orcid.org/0000-0001-5093-1549
Jay A Gupta https://orcid.org/0000-0002-3908-7719

References

[1] Roy S and Asenov A 2005 Where do the dopants go? *Science* **309** 388–90
[2] Shinada T, Okamoto S, Kobayashi T and Ohdomari I 2005 Enhancing semiconductor device performance using ordered dopant arrays *Nature* **437** 1128–31
[3] Lorenz J K, Asenov A, Baer E, Barraud S, Kluepfel F, Millar C and Nedjalkov M 2018 Process variability for devices at and beyond the 7 Nm node *ECS J. Solid State Sci. Technol.* **7** P595–601
[4] Fuechsle M, Miwa J A, Mahapatra S, Ryu H, Lee S, Warschkow O, Hollenberg L C L, Klimeck G and Simmons M Y 2012 A single-atom transistor *Nat. Nanotechnol.* **7** 242–6
[5] Koenraad P M and Flatté M E 2011 Single dopants in semiconductors *Nat. Mater.* **10** 91–100
[6] Kitchen D, Richardella A, Tang J-M, Flatté M E and Yazdani A 2006 Atom-by-Atom substitution of Mn in GaAs and visualization of their hole-mediated interactions *Nature* **442** 436–9
[7] Lee D H and Gupta J A 2010 Tunable field control over the binding energy of single dopants by a charged vacancy in GaAs *Science* **330** 1807–10
[8] Marczinowski F, Wiebe J, Meier F, Hashimoto K and Wiesendanger R 2008 Effect of charge manipulation on scanning tunneling spectra of single Mn acceptors in InAs *Phys. Rev.* B **77** 115318
[9] Teichmann K, Wenderoth M, Loth S, Ulbrich R, Garleff J, Wijnheijmer A and Koenraad P 2008 Controlled charge switching on a single donor with a scanning tunneling microscope *Phys. Rev. Lett.* **101** 076103
[10] Bocquel J, Kortan V R, Şahin C, Campion R P, Gallagher B L, Flatté M E and Koenraad P M 2013 Core-state manipulation of single Fe impurities in GaAs with a scanning tunneling microscope *Phys. Rev.* B **87** 075421
[11] Lee D-H and Gupta J A 2011 Tunable control over the ionization state of single Mn acceptors in GaAs with defect-induced band bending *Nano Lett.* **11** 2004–7
[12] Morgenstern M, Haude D, Gudmundsson V, Wittneven C, Dombrowski R and Wiesendanger R 2000 Origin of Landau oscillations observed in scanning tunneling spectroscopy on N-InAs(110) *Phys. Rev.* B **62** 7257–63
[13] Labidi H, Taucer M, Rashidi M, Koleini M, Livadaru L, Pitters J, Cloutier M, Salomons M and Wolkow R A 2015 Scanning tunneling spectroscopy reveals a silicon dangling bond charge state transition *New J. Phys.* **17** 073023
[14] Livadaru L, Pitters J, Taucer M and Wolkow R A 2011 Theory of nonequilibrium single-electron dynamics in STM imaging of dangling bonds on a hydrogenated silicon surface *Phys. Rev.* B **84** 205416
[15] Taucer M, Livadaru L, Piva P G, Achal R, Labidi H, Pitters J L and Wolkow R a 2014 Single-electron dynamics of an atomic silicon quantum dot on the H − Si(100) − (2 × 1) surface *Phys. Rev. Lett.* **112** 256801
[16] Rashidi M, Lloyd E, Huff T R, Achal R, Taucer M, Croshaw J J and Wolkow R A 2017 Resolving and tuning carrier capture rates at a single silicon atom gap state *ACS Nano* **11** 11732–8
[17] Schofield S R, Studer P, Hirjibehedin C F, Curson N J, Aeppli G and Bowler D R 2013 Quantum engineering at the silicon surface using dangling bonds *Nat. Commun.* **4** 1649
[18] Pradhan N a, Liu N, Silien C and Ho W 2005 Atomic scale conductance induced by single impurity charging *Phys. Rev. Lett.* **94** 076801
[19] Brar V W *et al* 2010 Gate-controlled ionization and screening of cobalt adatoms on a graphene surface *Nat. Phys.* **7** 43–7
[20] Song C-L, Jiang Y-P, Wang Y-L, Li Z, Wang L, He K, Chen X, Ma X-C and Xue Q-K 2012 Gating the charge state of single Fe dopants in the topological insulator Bi_2Se_3 with a scanning tunneling microscope *Phys. Rev.* B **86** 045441
[21] Zheng H, Kröger J and Berndt R 2012 Spectroscopy of single donors at ZnO(0001) surfaces *Phys. Rev. Lett.* **108** 076801
[22] Kaplan R 1969 Optical spectra of donor impurities in InSb in high magnetic fields *Phys. Rev.* **181** 1154–62
[23] Madelung O (ed) 1996 *Semiconductors—Basic Data* 2nd edn (Berlin: Springer)
[24] Grafström S 2002 Photoassisted scanning tunneling microscopy *J. Appl. Phys.* **91** 1717–53
[25] Blöchl P E 1994 Projector augmented-wave method *Phys. Rev.* B **50** 17953–79
[26] Kresse G 1996 *Ab initio* molecular dynamics applied to the dynamics of liquid metals and to the metal-non-metal transition *J. Non-Cryst. Solids* **205–207** 833–40
[27] Kresse G and Hafner J 1993 *Ab initio* molecular dynamics for liquid metals *Phys. Rev.* B **47** 558–61
[28] Bader R F 1994 *Atoms in Molecules: A Quantum Theory* (Oxford: Clarendon Press)

[29] Henkelman G, Arnaldsson A and Jónsson H 2006 A fast and robust algorithm for Bader decomposition of charge density *Comput. Mater. Sci.* **36** 354–60
[30] Sanville E, Kenny S D, Smith R and Henkelman G 2007 Improved grid-based algorithm for Bader charge allocation *J. Comput. Chem.* **28** 899–908
[31] Tang W, Sanville E and Henkelman G 2009 A grid-based Bader analysis algorithm without lattice bias *J. Phys.: Condens. Matter.* **21** 084204
[32] Tersoff J and Hamann D R 1985 Theory of the scanning tunneling microscope *Phys. Rev.* B **31** 805–13
[33] p4vasp 2021 The VASP visualization tool www.p4vasp.at
[34] Whitman L J, Stroscio J A, Dragoset R A and Celotta R J 1990 Scanning-tunneling-microscopy study of InSb(110) *Phys. Rev.* B **42** 7288–91
[35] Yang J, Nacci C, Martínez-Blanco J, Kanisawa K and Fölsch S 2012 Vertical manipulation of native adatoms on the InAs(111)A surface *J. Phys.: Condens. Matter.* **24** 354008
[36] Fölsch S, Yang J, Nacci C and Kanisawa K 2009 Atom-by-atom quantum state control in adatom chains on a semiconductor *Phys. Rev. Lett.* **103** 096104
[37] Kanisawa K and Fujisawa T 2008 Mechanism of electron accumulation layer formation at the MBE-grown InAs(111)A surface *Hyomen Kagaku* **29** 747–57
[38] Gohlke D, Mishra R, Restrepo O D, Lee D, Windl W and Gupta J 2013 Atomic-scale engineering of the electrostatic landscape of semiconductor surfaces *Nano Lett.* **13** 2418–22
[39] Khajetoorians A A, Chilian B, Wiebe J, Schuwalow S, Lechermann F and Wiesendanger R 2010 Detecting excitation and magnetization of individual dopants in a semiconductor *Nature* **467** 1084–7
[40] Zheng J F, Liu X, Newman N, Weber E R, Ogletree D F and Salmeron M 1994 Scanning tunneling microscopy studies of Si donors (SiGa) in GaAs *Phys. Rev. Lett.* **72** 1490–3
[41] Yoshida S, Aizawa Y, Wang Z-H, Oshima R, Mera Y, Matsuyama E, Oigawa H, Takeuchi O and Shigekawa H 2014 Probing ultrafast spin dynamics with optical pump-probe scanning tunnelling microscopy *Nat. Nanotechnol.* **9** 588–93
[42] Feenstra R M 2003 Electrostatic potential for a hyperbolic probe tip near a semiconductor *J. Vac. Sci. Technol.* B **21** 2080
[43] Stroscio J A and Feenstra R M 1988 Scanning tunneling spectroscopy of oxygen adsorbates on the GaAs(110) surface *J. Vac. Sci. Technol.* B **6** 1472–8
[44] Hashimoto K, Sohrmann C, Wiebe J, Inaoka T, Meier F, Hirayama Y, Römer R A, Wiesendanger R and Morgenstern M 2008 Quantum Hall transition in real space: from localized to extended states *Phys. Rev. Lett.* **101** 256802
[45] Morgenstern M, Getzlaff M, Haude D, Wiesendanger R and Johnson R L 2000 Coverage dependence of the Fe-induced Fermi-level shift and the two-dimensional electron gas on InAs(110) *Phys. Rev.* B **61** 13805–12
[46] Van de Walle C G and Neugebauer J 2003 Universal alignment of hydrogen levels in semiconductors, insulators and solutions *Nature* **423** 626–8
[47] Hjalmarson H P, Vogl P, Wolford D J and Dow J D 1980 Theory of substitutional deep traps in covalent semiconductors *Phys. Rev. Lett.* **44** 810–3
[48] Feenstra R M 1994 Tunneling spectroscopy of the (110) surface of direct-gap III–V semiconductors *Phys. Rev.* B **50** 4561–70
[49] Rashidi M, Burgess J A J, Taucer M, Achal R, Pitters J L, Loth S and Wolkow R A 2016 Time-resolved single dopant charge dynamics in silicon *Nat. Commun.* **7** 13258